SAND2020-5696J

Palladium-Coated Platinum Powders with Tunable, Nanostructured Surfaces for Applications in Catalysis

Sita Gurung[§], *David B. Robinson*[‡] *and Patrick J. Cappillino*[§,*]

[§]Department of Chemistry and Biochemistry, University of Massachusetts Dartmouth, Dartmouth, Massachusetts, United States

[‡]Energy Nanomaterials Department, Sandia National Laboratories, Livermore, California, United States

*pcappillino@umassd.edu

Keywords: ALD, ALED, Electroless, Surface Alloy, Growth mechanism, Galvanic Replacement, Surface Hydride, SLRR

Abstract

Simultaneous control of nanoscale surface morphology and composition remains a challenge in preparing bimetallic catalysts, particularly at the large scale required for industrial application, and with high surface area substrates. Atomic Layer Electroless Deposition (ALED) is a scalable approach to prepare surface-modified metal powders in which elements more noble than the surface hydrides of the substrate metal are deposited layer-by-layer in

surface-limited fashion. Herein we demonstrate that high surface area Pt powder is a viable substrate for controlled deposition of Pd adlayers using this technique, with the potential for large-scale preparation, for use in electrocatalytic and catalytic applications such as fuel cells and functionalization of petrochemical feedstocks. Two different growth mechanisms have been proposed based on bulk and surface Pd atomic fractions obtained from atomic absorption spectroscopy and X-ray photoelectron spectroscopy respectively. Further, spectral simulations were performed to strengthen the proposed growth mechanisms, favoring conformal growth in initial deposition followed by island formation in subsequent cycles. Observation of multiple pathways suggest a means of controlling adlayer surface morphology of ALED materials, in which an initial cycle of deposition sets the fractional coverage and subsequent cycles tune adlayer thickness.

Introduction

Surface and near-surface alloys of Pt have been reported to improve the catalytic properties of Pt catalyst, having wide range of applications in catalysis and electrocatalysis.[1-3] For example, presence of a subsurface layer of Ni on a Pt catalyst has shown to increase oxygen reduction activity by 10-fold over the Pt alone.[4] Further, a Pd overlayer on Pt catalyst acts to mitigate surface-poisoning during formic acid oxidation.[5] Many methods have been developed to prepare such bimetallic materials, most commonly wet-impregnation[6-9] and Atomic Layer Deposition (ALD).[10-12] While the former strategy lacks compositional control, in the latter case, self-limiting reactions afford tunable, atomically thin adlayers even in the case of high aspect-ratio substrates.[13-14] Disadvantages to conventional, gas-phase ALD include necessity for high-

temperature and ultra-high vacuum conditions as well as a reliance on volatile precursors and low coverage per cycle.[15-16]

In addition to the conventional methods of preparing bimetallic materials, discussed above, electrochemical atomic layer deposition (e-ALD) is an approach in which a sacrificial layer, such as Cu or Pb, is deposited on a substrate that is then galvanically displaced by an adlayer metal of interest.[17-21] It has also been demonstrated a sacrificial hydride layer can be formed electrochemically.[22-24] More recently, a technique that is complementary to e-ALD, known as electroless ALD, has received attention for several reasons. First, since it is carried out with solution-phase reagents rather than electrochemically, at the surface of a working electrode, it does not require the high power that would be required for electrodeposition on high-surface-area substrates. This factor also improves scalability over electrochemical methods. Furthermore, in contrast to e-ALD, the substrate does not need to be conductive in the case of electroless deposition. One recent example of this approach involves leveraging the reducing power of solution-phase V^{2+} ions to form monolayers of Pb, which are limited to the surface of the metal substrate.[25] These sacrificial Pb layers can then be galvanically replaced with the adlayer element of choice. In another example of electroless atomic layer deposition, a Pb auxiliary electrode is used to form monolayer deposits on a substrate working electrode without the need for a power source.[26]

While each of these approaches possesses a number of advantages, a means of preparing bimetallic materials in which the atoms present within a few nanometers of the surface are well-controlled, ***that can be carried out at the scale necessary for applications in catalysis***

and electrocatalysis, remains an important research goal. Recently, a method of atomic layer electroless deposition (ALED) was reported that shows excellent compositional control, and, since the process is chemical rather than electrochemical, it is amenable to large-scale implementation (Scheme 1).[27] It builds upon prior work using metal hydrides that grow overlayers upon themselves.[28] In ALED, elements more noble than the surface hydrides of the substrate metal are deposited layer-by-layer in surface-limited fashion. The substrate is first charged with a controlled partial pressure of H_2 gas to chemically form a surface hydride. After terminating the flow of reagent gas, surface-limited reduction of an adlayer of a different metal is carried out by galvanic exchange of the surface hydride. The process can be repeated to grow thicker films of varying composition. ALED is a robust, scalable approach offering simultaneous control of surface morphology and composition to obtain a conformal growth on high surface area substrates. In comparison with the methods described above, it combines the favorable attributes of nanoscale compositional control, scalability and a benign and easily removed hydride sacrificial layer that does not introduce contaminants to the prepared materials, such as Cu or Pb.

In previous studies, ALED has been carried out on Pd powder and Pd/C substrates.[27] Formation of a sacrificial metal hydride was limited to the surface of the substrate by controlling the partial pressure of hydrogen gas in nitrogen gas diluent, making use of the well-known thermodynamics of hydrogen absorption in Pd. Herein we demonstrate that this technique is not limited to Pd substrates and that the scope of ALED includes Pt as a substrate, with Pd as an adlayer metal. We describe details on the formation and stability of platinum

surface hydrides, which act as precursors for the galvanic replacement reaction.[29] These sacrificial hydrides are limited to a single surface-equivalent during each cycle. Further, controlled adlayer deposition was carried out with varying numbers of cycles. A growth model for deposition is proposed, based on comparison of bulk atomic fractions of Pd and Pt obtained from atomic absorption spectroscopy (AAS), versus surface atomic fractions obtained from X-ray photoelectron spectroscopy (XPS). These observations are strengthened by spectral simulations of three plausible surface morphologies that would result from conformal and three-dimensional modes of adlayer deposition.

Experimental

Materials

Palladium powder, (0.35-0.8-micron, 99.95% metal basis), platinum powder (< 3 micron, 99.9% metal basis), palladium wire (0.4 mm diameter, 99.9% metal basis), platinum wire (0.404 mm, diameter 99.9% metal basis) and sulfuric acid (99.999%) were purchased from Alfa Aesar. Potassium tetrachloropalladate was purchased from Strem Chemicals. Reagent gas (1% H_2 in N_2 was purchased from Praxair. All solutions were prepared with 18 MΩ•cm deionized water. Reference electrodes (RE), Ag/AgCl in 3 M NaCl were obtained from BASI and stored in vial containing 3 M NaCl.

Physical Methods

All electrochemistry was carried out using a Versastat 3 potentiostat (Ametek). Ag/AgCl (3M NaCl) and Pt wire were used as reference electrode (RE) and counter electrode (CE). A Pd or Pt electrode was chosen as working electrode (WE) depending upon the substrate used.

All the potential readings reported were taken with respect to Ag/AgCl RE (3 M NaCl). The open-circuit potential (OCP) referred to hereafter is the potential of the working electrode relative to the reference electrode with no potential or current applied to the cell. At the start of each experiment, the potential of the reference electrode was checked by comparison with a pristine standard reference electrode Ag/AgCl 3M NaCl.

ALED method

A 50 mL 3-neck cell ("ALED cell") was filled with 35 mL of 0.1 M H_2SO_4 and purged with N_2 prior to initial CV of WE Pt wire. The cell was then charged with 100 mg of Pt powder substrate and placed under efficient stirring. OCP was monitored for each ALED cycle, during an initial purge with nitrogen, while reagent gas was flowed through the cell to effect surface hydride formation, and to maintain headspace composition during adlayer deposition. A flow rate of 4 mL/s was used, except where otherwise indicated, during purge and reagent gas flow. A near zero flow rate with controlled flow of nitrogen was used during deposition to maintain the cell under slight, static, positive pressure. Subsequent to hydride formation, the cell was left to maintain static pressure for 5 min. prior to addition of adlayer solution. The adlayer K_2PdCl_4 stock solution was purged with nitrogen for half an hour prior to use. Aliquots of K_2PdCl_4 (0.25 mL or 0.5 mL, 2.46 mM~9.5 mM) were added depending upon the desired coverage of adlayer metal on substrate powder. For multiple cycles of ALED, the cell was once again purged with reagent gas to establish a stable hydride potential followed by addition of adlayer metal salt. After deposition, the prepared bimetallic materials (Pt*Pd*) were filtered,

rinsed several times with deionized water and dried over night at room temperature under reduced pressure.

Product characterization

Cyclic voltammetry (CV) of Pt or Pd wire was carried out in the ALED cell with 35 mL of 0.1 M H_2SO_4 as electrolyte. CV of Pt powder substrates and Pt*Pd* powder samples were performed in a custom-made, Teflon electrochemical cell shown in Figure S1 of the Supporting Information. A gold-plated slide placed in between Teflon blocks was used as WE, on which 10-15 mg of powder sample was placed. The powder was held in contact with the WE by pressing Fisher brand P8 grade filter paper with a Viton O-ring having 1.8 cm and 1.4 cm as outer and inner diameter respectively. The filter paper was prepared to have diameter slightly bigger than inner diameter but smaller than outer diameter of O-ring to avoid leaking of electrolyte. Sulfuric acid electrolyte (1 mL, 0.1 M) was subsequently introduced to the cell carefully to ensure no air bubbles were trapped in filter paper. The system was sealed with a septum and threaded with RE and CE by using a hollow leather punch set of respective appropriate size. The inlet and outlet gas tubing were accompanied by an 18-gauge BD precision glide needle. The system was purged with nitrogen before analysis and measurements were carried out. The scan rate used was 1 mV/s. This slow scan-rate was used to compare CVs of powder samples (compared with 100 mV/s scan rate for wire electrodes) because the surface area of powder electrodes in several orders of magnitude higher than that of the wire.

Surface analysis was performed by X-ray photoelectron spectrometry (XPS) at the Material Characterization Laboratory in University of Massachusetts Lowell with a VG Scientific

ESCALAB MKII using Mg Kα source with a photon energy of 1250 eV. The software program Casa XPS was used to integrate the area under the peaks after background subtraction to quantify the atomic concentration of metals present on surface. The software program Simulation of Electron Spectra for Surface Analysis (SESSA)[30] was used to simulate XPS spectra with various surface morphologies. The atomic concentration was calculated by dividing intensity of peaks with respective peak relative sensitivity factors (RSF values).[31-32] The simulated peaks were obtained using default setups describing conformal and island formation growth of Pd on Pt substrate.

The bulk concentration of deposited Pd in ALED prepared materials was quantified by atomic absorption spectrometry (AAS) using Perkin Elmer AAnalyst 100.

BET surface area[33] measurements were performed using a Micromeritics ASAP 2020 porosimeter. Nitrogen gas at 77 K was used as the adsorptive, and samples were degassed for 15 h at 50 °C prior to analysis.

Scanning electron microscopy (SEM) was carried out using a Hitachi SU5000 field-emission electron microscope with the powder samples sprinkled onto carbon tape.

Results and Discussion

Pt as a substrate for ALED:

Prior to powder deposition experiments, the dynamics of hydride formation on Pd and Pt wire were investigated (Figure 1). While differences between the behavior of a polycrystalline Pt wire and a polycrystalline Pt powder are to be expected, due to the much lower surface area and statistically differing distribution of crystallographic faces,[34] these experiments provide a

useful framework for understanding the ALED process. The response of the OCP in the first 15 minutes reflects changes at the surface of the Pt WE after a 5 min purge of N_2 gas, followed by introduction of reagent gas. Flow of dilute hydrogen gas in nitrogen carrier gas causes: (i) reduction of oxide present on the surface of Pt substrate which is shown by a steep fall in potential followed by (ii) formation of surface hydrides shown by a plateau of stable potential (~ -0.2 V vs Ag/AgCl). For Pt wire and Pd wire, the potential stabilized at -0.22 V and at -0.18 V respectively, presumably due to differences in surface hydride energetics.[35] In the case of Pd wire, the OCP is stable during N_2 purge at 4 mL/s flow rate while in case of Pt wire, the potential increases rapidly with time at the same N_2 flow rate, demonstrating that hydrides formed on the surface of Pt wire are more readily consumed than those formed on the Pd wire due to differences in surface-, subsurface and interstitial-hydride quantities and energetics.[36-37] An alternate hypothesis is that, in the case of Pd, dilute hydride formed in the bulk is slow to desorb. Nevertheless, these experiments confirmed that surface hydrides of Pt are sufficiently stable to persist for tens of minutes at low N_2 flow rates (green line, Figure 1) and for the duration of the experiment at static pressure (red line, Figure 1) facilitating galvanic displacement by Pd^{2+}.

In contrast to the slow increase in OCP under nitrogen flow, an immediate increase was observed when an aliquot of excess K_2PdCl_4 (2.46 mM, 0.25 mL) was introduced (blue line, Figure 1) indicating the consumption of surface hydride and presence of excess Pd^{2+} in solution after galvanic reduction of Pd^{2+} to Pd^0 by Pt-H. These experiments, in which Pt wire serves as a proxy for the Pt powder substrate, lay the groundwork for an ALED process in

which adlayer deposition is limited to one surface equivalent (SE) by i) placing the cell under static pressure of H_2/N_2 gas in each cycle, after hydride formation and before addition of the adlayer metal salt and ii) keeping the dose size to ≤ one SE of adlayer metal salt.

Stoichiometry for the deposition of one monolayer (ML) of Pd metal on Pt powder substrate:

Understanding the stoichiometry involved in galvanic replacement of PtH by reduction of Pd^{2+} ions during ALED cycles is a key aspect of controlling surface composition. An initial hypothesis, assuming a 2:1 surface PtH:Pd^{2+} stoichiometry, would provide a maximum possible surface coverage of ½ SE (equation 1).

$$2\,Pt-H+Pd^{2+}\rightarrow PtPd+Pt^{0}+2H^{+} \quad (1)$$

Given the measured BET surface area of the Pt powder used in these experiments of 5.2 m^2/g and the density of surface atoms in polycrystalline Pt of $1.31*10^{15}$ cm^{-2},[38-39] the expected ratio of surface Pt atoms to bulk Pt atoms can be approximated as 2.2×10^{-2}. Since Pt-H is expected to form at a 1:1 ratio with surface atoms[39], this also provides the ratio of surface hydrides formed to the total number of moles of Pt substrate atoms. Based on these considerations, one SE is defined as 22 mmol of surface atoms for one mol of total polycrystalline Pt powder substrate atoms. Correspondingly, one full surface equivalent of Pd^{2+} should results in 1.2% wt% Pd.

An OCP curve during an ALED titration of Pd powder, carried out to assess this hypothesis, is shown in Figure 2. In a manner similar to that described for the Pt wire, five minutes of N_2 purge is followed by exposure to reagent gas (1% H_2/N_2). The exposure of hydrogen gas in the

ALED system reduces the oxides present on the surface of Pt powder which is shown by gradual decrease in potential with time reaching to a plateau at the end. Potential stabilizes at -0.2 V due to formation of surface hydrides. The time required to reduce the surface oxides for Pt powder is much higher than that of Pt wire, due to its higher surface area. With addition of each aliquot (0.25 mL, 2.46 mM K_2PdCl_4), the potential rises due to galvanic replacement of surface hydride by adlayer metal as Pd^0 is deposited. The width of the orange box in Figure 2 corresponds to the number of aliquots resulting in one SE of Pd deposited based on the cumulative amount of Pd^{2+} added. The OCP is expected to increase more steeply with addition of Pd^{2+} once all surface hydrides have been consumed, and Pd^{2+} accumulates in the cell. These data suggest that Pd^{2+} deposits at a ~1:1 Pd:Pt stoichiometry, rather than the expected 1:2 stoichiometry, indicating the presence of reducing equivalents beyond those formed in 1:1 surface hydride formation. This observation agrees with the bulk concentration of Pd in this sample, as determined by AAS, of 1.30 wt% (Figure 3), which is very close to the theoretical expectation for one SE of Pd deposition. To understand this large departure from the expected stoichiometry several factors have been considered. First, physisorbed hydrogen, subsurface and subsurface-interstitial hydrogen present in Pt substrate are not expected to contribute appreciably to the amount of reducing equivalents.[29,40-43] Second, there may be some uncertainty in our estimate of the powder surface area and literature values for density of surface Pd and H atoms. Third, literature reports of solubility of hydrogen gas in the electrolyte should limit its concentration to less than 0.05 SE.[44] Finally, we estimate the amount of hydrogen in the headspace to be about 0.5 SE and it is reasonable to expect that much of this

will find its way to the powder surface on the timescale of the reaction. Overall, it is not surprising that one SE of Pd is deposited when a single cycle of hydride formation is followed by titration with Pd^{2+}. The presence of headspace hydrogen is potentially helpful in preventing loss of surface hydride to side reactions, but this result highlights the need to manage its quantity carefully.

ALED of Pd on Pt powder:

Based on the surface area of the Pt substrate and titration experiments above, the aliquot of adlayer metal salt added to prepared surface hydrides during each ALED was below one theoretical SE. This prevents accumulation of the metal salt in the electrolyte with successive cycles. In this way, deposition of Pd^0 by direct interaction with hydrogen gas in a manner not limited to the surface of the substrate was avoided. For these experiments, adlayer Pd^{2+} solution was prepared to deposit 0.43 SE of Pd (0.5 mL of 9.5 mM K_2PdCl_4 for 0.1 g of Pt) per cycle. OCP traces of one-cycle and three-cycle deposition of Pd on Pt powder are shown in Figure 4. The flow of reagent gas was terminated and the adlayer metal salt was introduced under static pressure of N_2, causing the potential to increase with the galvanic displacement of surface PtH to reduce Pd^{2+} to Pd^0. For multiple ALED cycles, the reagent gas was again introduced to form surface hydrides followed by addition of an adlayer metal aliquot. Consistent increase in potential was obtained in successive cycles of the same size aliquot, strongly suggesting a similar quantity of surface hydrides are consumed. The maximum OCP observed in each cycle was < -0.1 V, suggesting all Pd^{2+} was consumed in the galvanic replacement reaction.

The SEM of Pt powder substrate before and after ALED (Figure 5) indicates no change in morphology due to the deposition process at the scale of several nanometers. Consistent with previous reports of ALED materials[27] there is no evidence of dendrites larger than a few nanometers.

The bulk concentration of deposited Pd was determined using AAS for three samples with 1, 2 and 3 cycles of ALED and was consistent with the increase in number of cycles, as shown by linear plot in Figure 3. These results, obtained on samples that were completely digested in nitric acid prior to analysis, are consistent with expectations for the total amount of Pd added to 100 mg of Pt powder substrate (Figure 3, inset). The efficiency of deposition observed here compares favorably to conventional ALD, in which many nucleation cycles are often necessary, with the quantity deposited per cycle is substantially lower.[16]

The AAS data above confirms a linear increase in total Pd concentration with each cycle of ALED. In contrast, XPS analysis (Figure 6) provides a surface-sensitive measure of Pd concentration. Since the mean-free path of both Pd and Pt photelectrons is between 1.5 and 2 nm, the atomic concentration at the surface of prepared ALED of Pd on Pt powder can be probed.[47] The Pd $3d_{5/2}$, Pd $3d_{3/2}$, Pt $4d_{5/2}$ and Pt $4d_{3/2}$ peaks were used to quantify the respective metal concentration on the surface. The atomic fraction of Pd was found to be 22% and 30% after deposition of 0.43 surface equivalents (one cycle) and 1.28 surface equivalents (three cycles), respectively. The large increase in atomic fraction Pd after the first cycle, followed by much smaller increases in subsequent cycles, in contrast to the monotonic increase in bulk Pd concentration measured by AAS, is indicative of a three-dimensional growth mechanism after

the initial deposition cycle. These data are consistent with conformal growth during initial deposition followed by island formation, as in the pseudomorphic Stranski-Krastanov mechanism, in which layer by layer growth of deposited metal dominates initially, followed by island growth after the formation of the first monolayer.[48-49]

The growth mechanism hypothesis above was further explored by comparing experimental data with simulated XPS spectra of various surface morphologies modeled with the Simulation of Electron Spectra for Surface Analysis (SESSA) software package.[30] Conformal Pd monolayers with a presumed thickness of 4 Å Pd on a Pt substrate with coverage ranging from 0.1 SE to 10 SE were simulated, along with island growth models in which, after an initial cycle of no more than one SE, additional adlayers deposit on previously deposited Pd metal instead of bare Pt substrate sites (Figure 7). The slope of increasing atomic fraction Pd for the 0.3 SE-island growth model is shallower than for 0.6 SE, which is shallower than for conformal deposition, since conformal deposition leads to a larger fraction of Pd atoms within the ~2 nm photoelectron mean free path.[47]

The experimentally determined 22% Pd after one cycle most closely matches the simulated conformal deposition of approximately 0.6 SE (Figure S2). On the other hand, after two additional cycles of equal aliquots, Pd atomic fraction has only increased by 8% to 30%. This most closely matches the simulation of two additional cycles of 0.6 SE deposition and is inconsistent with either conformal or 0.3 SE island deposition. While this represents strong evidence for three-dimensional growth in cycles two and three, we note that there is no direct experimental evidence for conformal growth during the first cycle, since initially only substrate

photoelectron attentuation can be observed. As such, though the simulated spectra are inconsistent with low fractional-coverage, high aspect-ratio growth (i.e., dendrites), some degree of three-dimensional growth in the first cycle cannot be ruled out. This proposed mechanism, in which the first deposition cycle sets the fractional coverage and subsequent cycles increase the adlayer thickness contrasts with that reported by recently by Dimitrov for the case of simultaneous H_{UPD}/ Pd SLRR.[23] In that case, a continuos monolayer forms by concomitant formation of the H_{UPD} layer and SLRR galvanic displacement by Pd ions.

Electrochemistry of Pt, Pt powder and bimetallic materials:

The electrochemistry of single crystal and polycrystalline Pt with different ratios of low index faces is well-established.[50-52] Similar to these previous results, the CV of Pt wire in dilute, N_2-purged sulfuric acid can be classified into three different potential ranges as shown in Figure 8a; A hydrogen adsorption(H_{ads}) /desorption (H_{des}) or H_{upd} region occurs between -0.2 V and 0 V vs Ag/AgCl, a double layer region is observed between 0 V and +0.25 V and oxidation/reduction of surface oxide occurs between 0.25 V and 1.2 V. In the positive, forward scan, oxidation of hydrogen occurs on the surface of Pt wire generating H^+ ions, showing anodic H_{des} peaks near -0.16 V and -0.06 V vs Ag/AgCl. In the negative, reverse scan, reduction of surface oxide occurs around +0.38 V followed by reduction of H^+ ion on Pt surface showing cathodic H_{des} peaks around -0.18 V and -0.07 V and eventually H_2 evolution at lower potentials. In the early literature, these H_{des}/H_{ads} peaks were referred to as H_w (-0.18 V) and H_s (-0.07 V) corresponding to weakly and strongly adsorbed hydrogen. More recently, they have been accepted to arise from hydrogen adsorption at different crystallographic faces of Pt.[53-54] The

cathodic/anodic peaks in CV of Pt wire near -0.18 V and -0.07 V are attributable to H_{des}/H_{ads} at Pt (110) and Pt (100), respectively, consistent with previous studies.[55]

CV of bulk Pt powder, on the other hand (Figure 8b), is not well-represented in the literature, and its interpretation exhibits great diversity, presumably as a result of high surface area, varying particle size, and variations in the statistical distribution of crystallographic faces.[34,52-53,56] In analogy to Pt wire, we assign the H_{ads}/H_{des} peak at the most negative potential (-0.2 V/-0.16 V) as Pt (110), whereas peaks near -0.13V/-0.08 V corresponds to Pt (100). The peak to the most positive potential is assigned to the more stable hydrides formed on Pt (111) at -0.03 V (Figure 8b).

After one cycle of ALED, the features in the CV of Pt powder attributable to H_{ads}/H_{des} on (110), (100) and (111) crystallographic faces, are diminished and broader (Figure 9). This result is similar to previously reported Pd on Pt NC eletcrodes,[55] and is consistent with coverage of Pt surface sites by Pd. Notably, the peak at highest potential, attributable to H_{ads}/H_{des} on the Pt(111) face, is completely absent after only one cycle of ALED, consistent with Pd deposition on the more stable H-UPD sites first. However, several features of the Pt surface are still evident, including a sharp feature at -0.17 V vs Ag/AgCl and several broad features. This is consistent with several distinct surface sites with differing M-H energetics. After three cycles of ALED, multiple features remain clearly evident, as the voltammogram gradually begins to resemble that of pure Pd (dotted line, Figure 9), with a broad desorption peak near -0.17 V vs AgCl. This is consistent with the spectroscopic analyses presented above, with an initial cycle

of incomplete conformal deposition, followed by cycles of increasing thickness of Pd and some remaining Pt sites.

Conclusions

The data presented herein demonstrate that Pd adlayers are efficiently deposited on Pt using ALED in a controlled, scalable fashion. Two different growth mechanisms are proposed and supported by surface and bulk spectroscopy, spectral simulations and cyclic voltammetry, raising the intriguing possibility of tunable surface stoichiometry. These analyses provide a unified picture, whereby conformal deposition of Pd occurs in the initial cycle, followed by island growth in subsequent cycles. This understanding lays the groundwork for preparation of bimetallic catalysts having low fractional coverage of alloying metals, for applications in which mitigation of surface poison adsorption is necessary,[57] for example, ***versus*** high fractional coverage, conformal adlayers for applications where modulation of ***d***-band energy is of interest.[58] Further, the chemical nature of sacrificial hydride layer formation in ALED renders it amenable to industrial-scale production of these nanostructured bimetallic catalysts. Future work will focus on investigating these growth mechanisms in more detail, controlling morphology by first setting fractional coverage and then tuning thickness with subsequent cycles, and in establishing surface-structure/function relationships by studying the reactivity of ALED catalysts.

Associated Content

Supporting Information

An electrochemical cell prepared to record CV of powders is shown in Figure S1. Simulated spectra for three growth models along with original XPS spectra of ALED prepared Pt*Pd* -1 cycle are shown in Figure S2.

Author Information

Corresponding Author

*Address: University of Massachusetts Dartmouth, 285 Old Westport Road, Dartmouth, MA, 02747, USA. E-mail: pcappillino@umassd.edu

Author Contributions

The manuscript was written through contributions of all authors. All authors have given approval to the final version of the manuscript.

Notes

All the authors declare no competing financial interest.

Funding sources

The electron microscopy images in this work were obtained using a scanning electron microscope supported by the National Science Foundation under Grant Number 1726239. This research was sponsored in part by the Army Research Laboratory under Grant Number W911NF-16-1-0438.

Acknowledgements

The electron microscopy images in this work were obtained using a scanning electron microscope supported by the National Science Foundation under Grant Number 1726239. This research was sponsored in part by the Army Research Laboratory under Grant Number W911NF-16-1-0438.

Sandia National Laboratories is a multimission laboratory managed and operated by National Technology & Engineering Solutions of Sandia, LLC, a wholly owned subsidiary of Honeywell International Inc., for the U.S. Department of Energy's National Nuclear Security Administration under contract DE-NA0003525. This paper describes objective technical results and analysis. Any subjective views or opinions that might be expressed in the paper do not necessarily represent the views of the U.S. Department of Energy or the United States Government.

References

1. Uhm, S.; Lee, H. J.; Kwon, Y.; Lee, J. A stable and cost-effective anode catalyst structure for formic acid fuel cells. *Angew. Chem. , Int. Ed.* 2008*, 47*, 10163-10166.

2. Lovic, J. D.; Stevanovic, S. I.; Tripkovic, D. V.; Tripkovic, V. V.; Stevanovic, R. M.; Popovic, K. D.; Jovanovic, V. M. Formic Acid Oxidation at Platinum-Bismuth Clusters. *J. Electrochem. Soc.* 2014*, 161*, H547-H554.

3. Gong, M.; Li, F.; Yao, Z.; Zhang, S.; Dong, J.; Chen, Y.; Tang, Y. Highly active and durable platinum-lead bimetallic alloy nanoflowers for formic acid electrooxidation. *Nanoscale* 2015*, 7*, 4894-4899.

4. Stamenkovic, V. R.; Fowler, B.; Mun, B. S.; Wang, G.; Ross, P. N.; Lucas, C. A.; Markovic, N. M. Improved Oxygen Reduction Activity on Pt3Ni(111) via Increased Surface Site Availability. *Science (Washington, DC, U. S.)* 2007, *315*, 493-497.

5. Lee, H.; Habas, S. E.; Somorjai, G. A.; Yang, P. Localized Pd Overgrowth on Cubic Pt Nanocrystals for Enhanced Electrocatalytic Oxidation of Formic Acid. *J. Am. Chem. Soc.* 2008, *130*, 5406-5407.

6. Konoshita, K.; Routsis, K.; Bett, J. A. S. Thermal decomposition of platinum(II) and (IV) complexes. *Thermochim. Acta* 1974, *10*, 109-117.

7. Brunelle, J. P. Preparation of catalysts by metallic complex adsorption on mineral oxides. *Pure Appl. Chem.* 1978, *50*, 1211-1229.

8. Zhang, Y.; Diao, W.; Williams, C. T.; Monnier, J. R. Selective hydrogenation of acetylene in excess ethylene using Ag- and Au-Pd/SiO2 bimetallic catalysts prepared by electroless deposition. *Appl. Catal. , A* 2014, *469*, 419-426.

9. De, S.; Zhang, J.; Luque, R.; Yan, N. Ni-based bimetallic heterogeneous catalysts for energy and environmental applications. *Energy Environ. Sci.* 2016, *9*, 3314-3347.

10. Christensen, S. T.; Elam, J. W. Atomic Layer Deposition of Ir-Pt Alloy Films. *Chem. Mater.* 2010, *22*, 2517-2525.

11. Lu, J.; Low, K.; Lei, Y.; Libera, J. A.; Nicholls, A.; Stair, P. C.; Elam, J. W. Toward atomically-precise synthesis of supported bimetallic nanoparticles using atomic layer deposition. *Nat. Commun.* 2014, *5*, 4264/1-4264/9.

12. Wang, H.; Luo, Q.; Liu, W.; Lin, Y.; Guan, Q.; Zheng, X.; Pan, H.; Zhu, J.; Sun, Z.; Wei, S.; Yang, J.; Lu, J. Quasi Pd1Ni single-atom surface alloy catalyst enables hydrogenation of nitriles to secondary amines. *Nat. Commun.* 2019, *10*, 1-9.

13. Lu, J.; Elam, J. W.; Stair, P. C. Atomic layer deposition-Sequential self-limiting surface reactions for advanced catalyst "bottom-up" synthesis. *Surf. Sci. Rep.* 2016, *71*, 410-472.

14. Lu, J.; Elam, J. W.; Stair, P. C. Synthesis and Stabilization of Supported Metal Catalysts by Atomic Layer Deposition. *Acc. Chem. Res.* 2013, *46*, 1806-1815.

15. Weber, M. J.; Mackus, A. J. M.; Verheijen, M. A.; Longo, V.; Bol, A. A.; Kessels, W. M. M. Atomic Layer Deposition of High-Purity Palladium Films from Pd(hfac)2 and H2 and O2 Plasmas. *J. Phys. Chem. C* 2014, *118*, 8702-8711.

16. Mackus, A. J. M.; Garcia-Alonso, D.; Knoops, H. C. M.; Bol, A. A.; Kessels, W. M. M. Room-temperature atomic layer deposition of platinum. *Chem. Mater.* 2013, *25*, 1769-1774.

17. Jayaraju, N.; Vairavapandian, D.; Kim, Y. G.; Banga, D.; Stickney, J. L. Electrochemical atomic layer deposition (E-ALD) of Pt nanofilms using SLRR cycles. *J. Electrochem. Soc.* 2012, *159*, D616-D622.

18. Sheridan, L. B.; Gebregziabiher, D. K.; Stickney, J. L.; Robinson, D. B. Formation of Palladium Nanofilms Using Electrochemical Atomic Layer Deposition (E-ALD) with Chloride Complexation. *Langmuir* 2013, *29*, 1592-1600.

19. Benson, D. M.; Tsang, C. F.; Sugar, J. D.; Jagannathan, K.; Robinson, D. B.; El Gabaly, F.; Cappillino, P. J.; Stickney, J. L. Enhanced Kinetics of Electrochemical Hydrogen Uptake and Release by Palladium Powders Modified by Electrochemical Atomic Layer Deposition. *ACS Appl. Mater. Interfaces* 2017, *9*, 18338-18345.

20. Dimitrov, N. Recent Advances in the Growth of Metals, Alloys, and Multilayers by Surface Limited Redox Replacement (SLRR) Based Approaches. *Electrochim. Acta* 2016, *209*, 599-622.

21. Brankovic, S. R.; Wang, J. X.; Adzic, R. R. Metal monolayer deposition by replacement of metal adlayers on electrode surfaces. *Surf. Sci.* 2001, *474*, L173-L179.

22. Nutariya, J.; Fayette, M.; Dimitrov, N.; Vasiljevic, N. Growth of Pt by surface limited redox replacement of underpotentially deposited hydrogen. *Electrochim. Acta* 2013, *112*, 813-823.

23. Achari, I.; Ambrozik, S.; Dimitrov, N. Electrochemical Atomic Layer Deposition of Pd Ultrathin Films by Surface Limited Redox Replacement of Underpotentially Deposited H in a Single Cell. *J. Phys. Chem. C* 2017, *121*, 4404-4411.

24. Liu, Y.; Gokcen, D.; Bertocci, U.; Moffat, T. P. Self-Terminating Growth of Platinum Films by Electrochemical Deposition. *Science (Washington, DC, U. S.)* 2012*, 338*, 1327-1330.

25. Wu, D.; Solanki, D. J.; Ramirez, J. L.; Yang, W.; Joi, A.; Dordi, Y.; Dole, N.; Brankovic, S. R. Electroless Deposition of Pb Monolayer: A New Process and Application to Surface Selective Atomic Layer Deposition. *Langmuir* 2018*, 34*, 11384-11394.

26. Ambrozik, S.; Rawlings, B.; Vasiljevic, N.; Dimitrov, N. Metal deposition via electroless surface limited redox replacement. *Electrochem. Commun.* 2014*, 44*, 19-22.

27. Cappillino, P. J.; Sugar, J. D.; El Gabaly, F.; Cai, T. Y.; Liu, Z.; Stickney, J. L.; Robinson, D. B. Atomic-Layer Electroless Deposition: A Scalable Approach to Surface-Modified Metal Powders. *Langmuir* 2014*, 30*, 4820-4829.

28. Wang, J. X.; Adzic, R. R. Patent Application Country: Application: US; US; Priority Application Country: US Patent US20060134505, 2006.

29. Martins, M. E.; Zinola, C. F.; Andreasen, G.; Salvarezza, R. C.; Arvia, A. J. The possible existence of subsurface H-atom adsorbates and H_2 electrochemical evolution reaction intermediates on platinum in acid solutions. *J. Electroanal. Chem.* 1998*, 445*, 135-154.

30. Smekal, W.; Werner, W. S. M.; Powell, C. J. Simulation of electron spectra for surface analysis (SESSA): A novel software tool for quantitative Auger-electron spectroscopy and X-ray photoelectron spectroscopy. *Surf. Interface Anal.* 2005*, 37*, 1059-1067, 2 plates.

31. Hill, S. B.; Faradzhev, N. S.; Powell, C. J. Quantitative analysis of trace levels of surface contamination by X-ray photoelectron spectroscopy. Part I: Statistical uncertainty near the detection limit. *Surf. Interface Anal.* 2017*, 49*, 1187-1205.

32. Faradzhev, N. S.; Hill, S. B.; Powell, C. J. Quantitative analysis of trace levels of surface contamination by X-ray photoelectron spectroscopy. Part II: Systematic uncertainties and absolute quantification. *Surf. Interface Anal.* 2017*, 49*, 1214-1224.

33. Brunauer, S.; Emmett, P. H.; Teller, E. Adsorption of gases in multimolecular layers. *J. Am. Chem. Soc.* 1938*, 60*, 309-319.

34. Van Hardeveld, R.; Hartog, F. Statistics of surface atoms and surface sites on metal crystals. *Surface Sci.* 1969*, 15*, 189-230.

35. Greeley, J.; Mavrikakis, M. Surface and Subsurface Hydrogen: Adsorption Properties on Transition Metals and Near-Surface Alloys. *J. Phys. Chem. B* 2005*, 109*, 3460-3471.

36. Lynch, J. F.; Flanagan, T. B. Dynamic equilibrium between chemisorbed and absorbed hydrogen in the palladium/hydrogen system. *J. Phys. Chem.* 1973*, 77*, 2628-2634.

37. Simons, J. W.; Flanagan, T. B. Absorption isotherms of hydrogen in the α-phase of the hydrogen-palladium system. *J. Phys. Chem.* 1965*, 69*, 3773-3781.

38. Trasatti, S.; Petrii, O. A. Real surface area measurements in electrochemistry. *J. Electroanal. Chem.* 1992*, 327*, 353-376.

39. Biegler, T.; Rand, D. A. J.; Woods, R. Limiting oxygen coverage on platinized platinum; relevance to determination of real platinum area by hydrogen adsorption. *J. Electroanal. Chem. Interfacial Electrochem.* 1971*, 29*, 269-277.

40. Lagos, M. Subsurface bonding of hydrogen to metallic surfaces. *Surf. Sci.* 1982*, 122*, L601-L607.

41. Christmann, K. Interaction of hydrogen with solid surfaces. *Surf. Sci. Rep.* 1988*, 9*, 163.

42. Zinola, C. F.; Arvia, A. J. A semiempirical quantum chemistry approach to possible structures and energies of hydrogen atoms adsorbed on Pt(100) and Pt(111) clusters at a simulated Pt/aqueous electrochemical interface. *Electrochim. Acta* 1996*, 41*, 2267-2273.

43. Ebisuzaki, Y.; Kass, W. J.; O'Keeffe, M. Solubility and diffusion of hydrogen and deuterium in platinum. *J. Chem. Phys.* 1968*, 49*, 3329-3332.

44. Ruetschi, P.; Amlie, R. F. Solubility of hydrogen in potassium hydroxide and sulfuric acid. Salting-out and hydration. *J. Phys. Chem.* 1966*, 70*, 718-723.

45. Homer, M.; Cappillino, P.; Gabaly, F.; Gnaegi, H.; Robinson, D.; Sugar, J. Preparation of Electron and X-Ray Transparent Inorganic Particles for Analytical Microscopy Using the Ultramicrotome. *Microscopy and Microanalysis* 2015*, 21*, 1815-1816.

46. Vitale, S.; Sugar, J.; Cappillino, P.; Giannuzzi, L.; Beljonne, D. Site Specific Preparation of Powders for High-Resolution Analytical Electron Microscopy Using a Ga+ Focused Ion Beam. *Microscopy and Microanalysis* 2016*, 22*, 180-181.

47. Powell, C. J.; Jablonski, A. Evaluation of Calculated and Measured Electron Inelastic Mean Free Paths Near Solid Surfaces. *J. Phys. Chem. Ref. Data* 1999, *28*, 19-62.

48. Ball, M. J.; Lucas, C. A.; Markovic, N. M.; Stamenkovic, V.; Ross, P. N. From sub-monolayer to multilayer - an in situ X-ray diffraction study of the growth of Pd films on Pt(111). *Surf. Sci.* 2002, *518*, 201-209.

49. Ball, M. J.; Lucas, C. A.; Markovic, N. M.; Stamenkovic, V.; Ross, P. N. Surface X-ray scattering studies of the growth of Pd thin films on the Pt(001) electrode surface and the effects of the adsorption of CO. *Surf. Sci.* 2003, *540*, 295-302.

50. Clavilier, J.; Faure, R.; Guinet, G.; Durand, R. Preparation of monocrystalline platinum microelectrodes and electrochemical study of the plane surfaces cut in the direction of the {111} and {110} planes. *J. Electroanal. Chem. Interfacial Electrochem.* 1980, *107*, 205-209.

51. Armand, D.; Clavilier, J. Electrochemical behavior of the (110) orientation of a platinum surface in acid medium. The role of anions. *J. Electroanal. Chem. Interfacial Electrochem.* 1989, *263*, 109-126.

52. Clavilier, J.; Llorca, M. J.; Feliu, J. M.; Aldaz, A. Preliminary study of the electrochemical adsorption behavior of a palladium modified platinum (111) electrode in the whole range of coverage. *J. Electroanal. Chem. Interfacial Electrochem.* 1991, *310*, 429-435.

53. Devivaraprasad, R.; Ramesh, R.; Naresh, N.; Kar, T.; Singh, R. K.; Neergat, M. Oxygen Reduction Reaction and Peroxide Generation on Shape-Controlled and Polycrystalline Platinum Nanoparticles in Acidic and Alkaline Electrolytes. *Langmuir* 2014, *30*, 8995-9006.

54. Llorca, M. J.; Feliu, J. M.; Aldaz, A.; Clavilier, J. Electrochemical structure-sensitive behavior of irreversibly adsorbed palladium on platinum(100), platinum(111) and platinum(110) in an acidic medium. *J. Electroanal. Chem.* 1993, *351*, 299-319.

55. Li, Y.; Wang, Z. W.; Chiu, C.; Ruan, L.; Yang, W.; Yang, Y.; Palmer, R. E.; Huang, Y. Synthesis of bimetallic Pt-Pd core-shell nanocrystals and their high electrocatalytic activity modulated by Pd shell thickness. *Nanoscale* 2012, *4*, 845-851.

56. Aran-Ais, R. M.; Solla-Gullon, J.; Herrero, E.; Feliu, J. M. On the quality and stability of preferentially oriented (100) Pt nanoparticles: An electrochemical insight. *J. Electroanal. Chem.* 2018, *808*, 433-438.

57. Zhang, Y.; Diao, W.; Williams, C. T.; Monnier, J. R. Selective hydrogenation of acetylene in excess ethylene using Ag- and Au-Pd/SiO2 bimetallic catalysts prepared by electroless deposition. *Appl. Catal. , A* 2014, *469*, 419-426.

58. Zhang, B.; Yang, H.; Wang, Y.; Dou, S.; Liu, H. A Comprehensive Review on Controlling Surface Composition of Pt-Based Bimetallic Electrocatalysts. *Adv. Energy Mater.* 2018, *8*, 5010-5016.

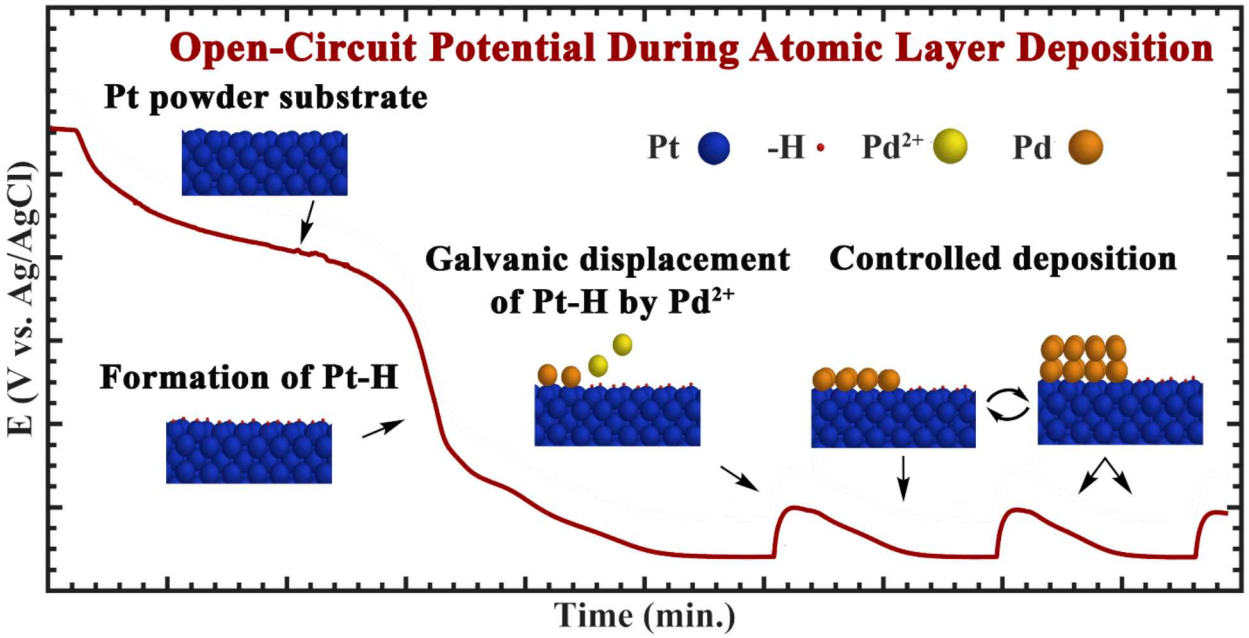

Table of Contents (TOC) graphic

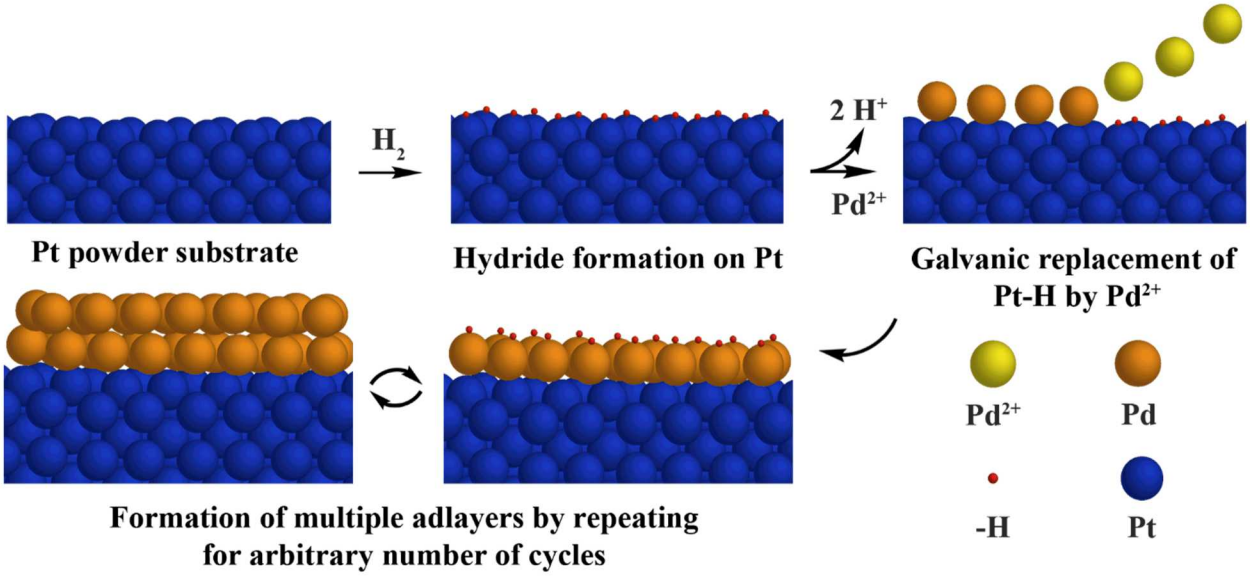

Scheme 1. Schematics of Atomic Layer Electroless Deposition (ALED) with Pt powder as substrate and Pd^{2+} as an adlayer metal.

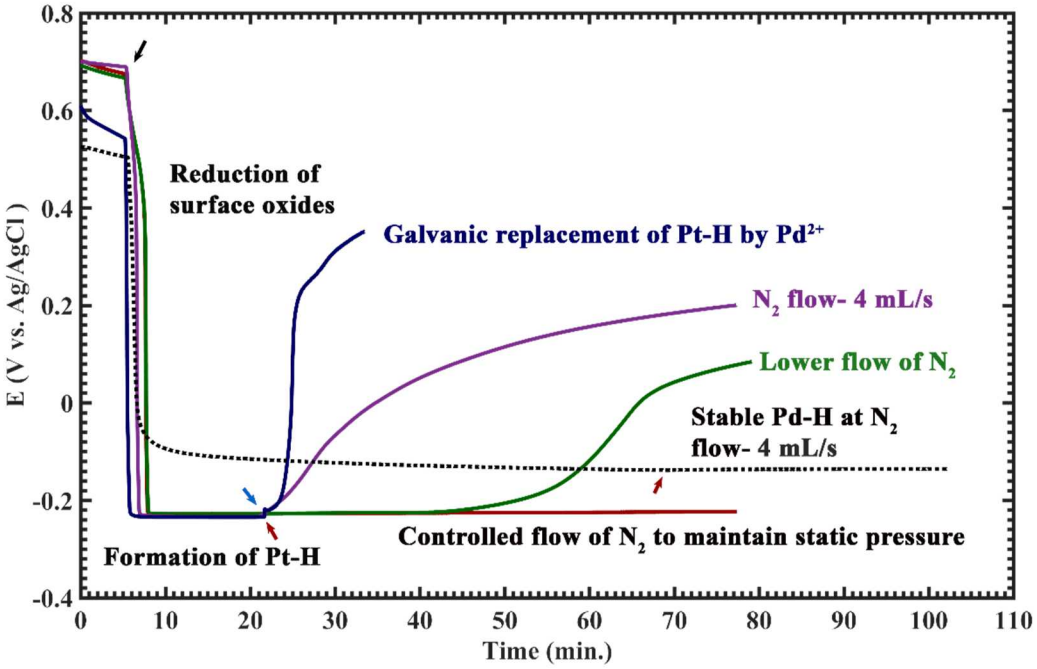

Figure 1. Comparative OCP of Pt wire (solid lines) and Pd wire (dashed line) at different conditions to study the stability of Pt-H. Different colored arrow signs are used to indicate the switching of gases which remains consistent throughout this paper; black arrow (switching from N_2 to 1% H_2/N_2), red (switching from 1% H_2/N_2 to N_2) and blue (adlayer metal aliquot addition).

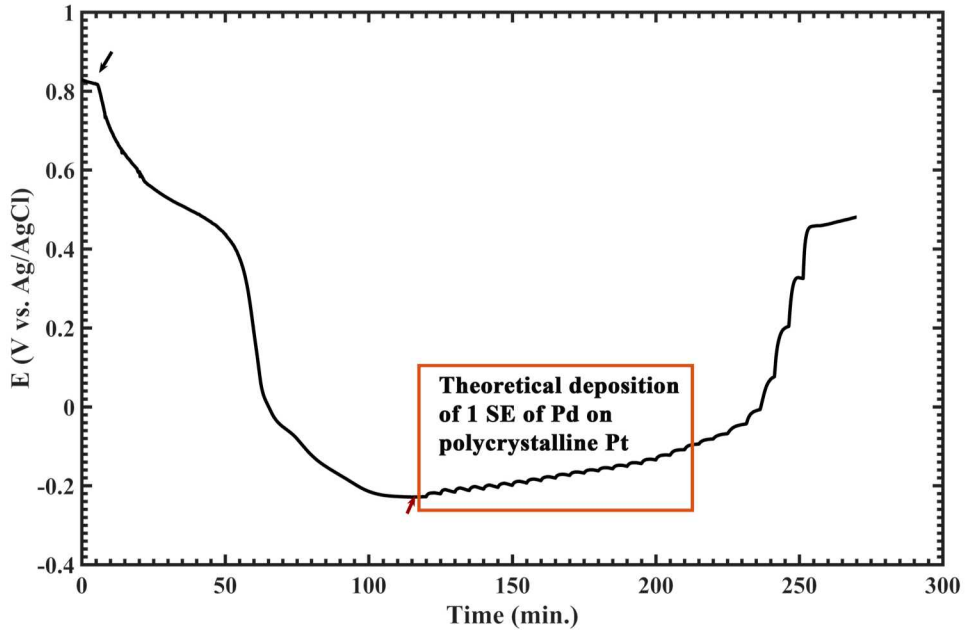

Figure 2. OCP of Pt powder titration to study maximum Pd depostion. The orange box indicates theoretical one SE of Pd deposited on polycrystalline Pt substrate.

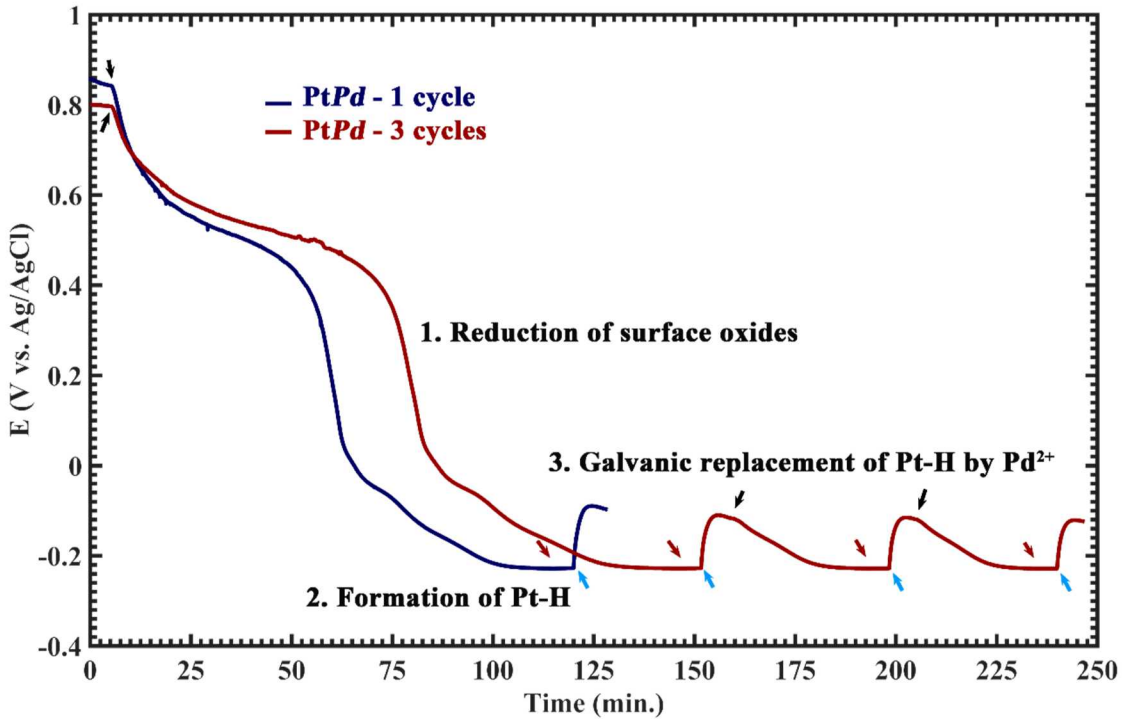

Figure 3. OCP traces of Pt*Pd* deposited by ALED for 1 cycle (blue) and 3 cycles (red).

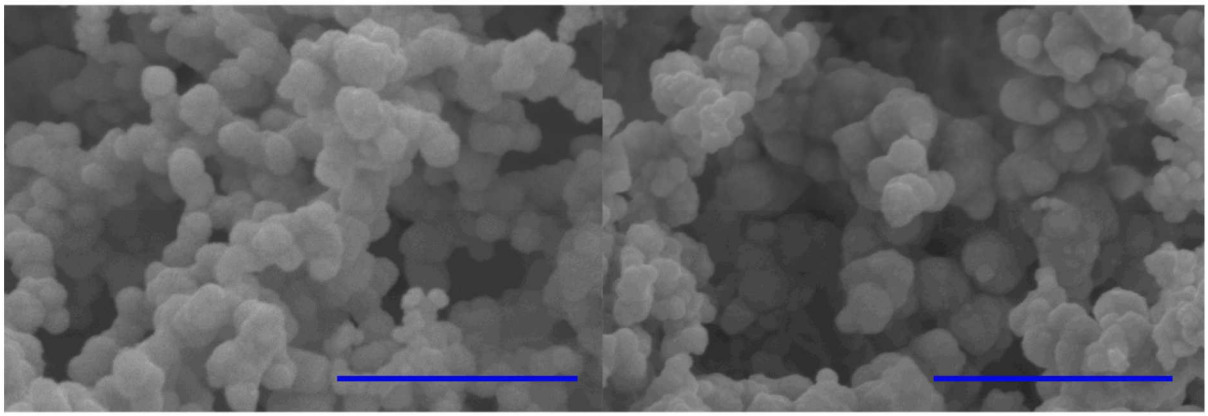

Figure 4. SEM images Pt substrate before ALED (left), after 3 cycles of ALED (right);

Scalebar = 500 nm.

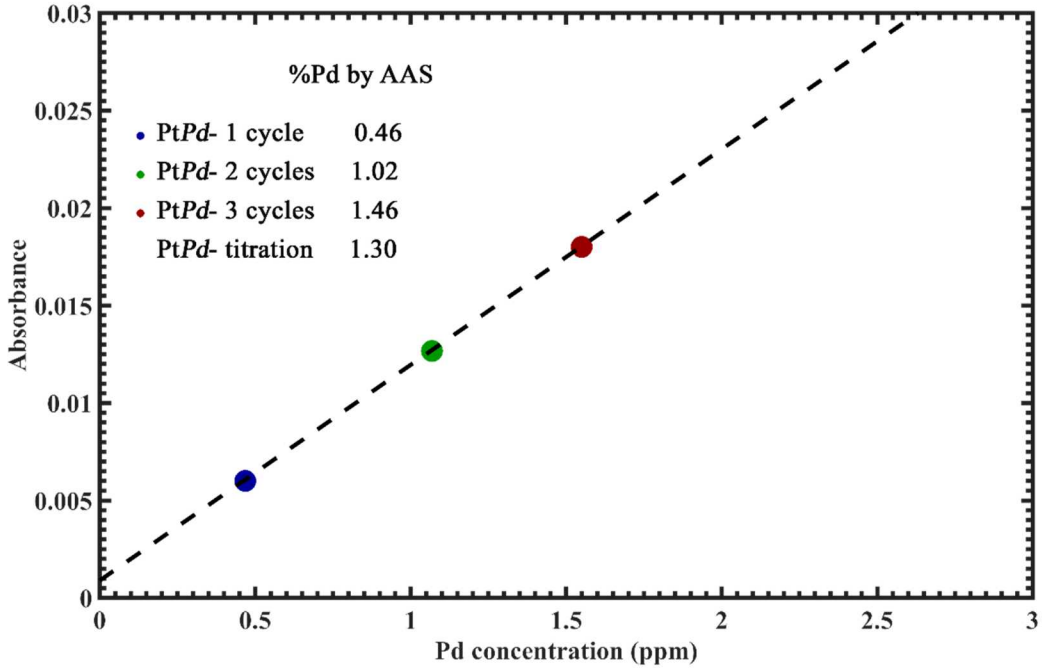

Figure 5. Atomic absorbance values of Pt*Pd* samples after one, two and three cycles of ALED. Five calibration points for AAS analysis were evenly distributed between 0 to 10 ppm and exhibited a linear response in this range (calibration data > 3 ppm not shown).

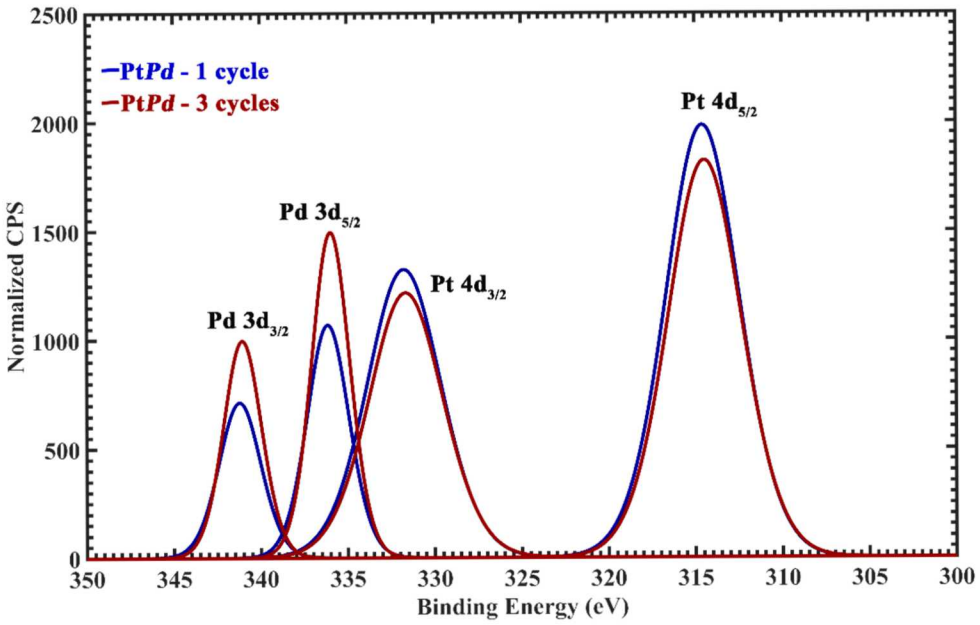

Figure 6. Normalized XPS spectra (fitted) for Pt*Pd* with 1 cycle and 3 cycles.

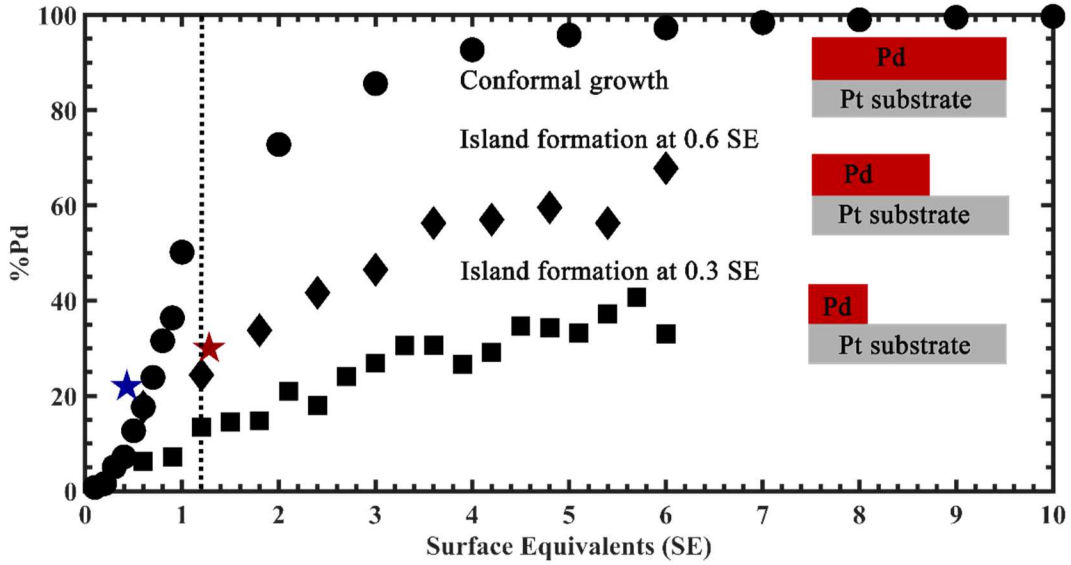

Figure 7. Simulated atomic concentration of Pd considering three scenarios; (a) 1. Conformal atomic (4Å) coverage of Pd ranging from 0.1 SE to 10 SE (circle), 2. Island formation with increasing number of 4Å layers covering 0.6 SE (diamond) and 3. Island formation with increasing number of 4Å layers covering 0.3 SE (square). Star signs give the XPS quantification of Pd of 1 cycle (blue-22% Pd) and 3 cycles (red-30% Pd). Inset: Schematics of one cycle of each ALED growth model considered.

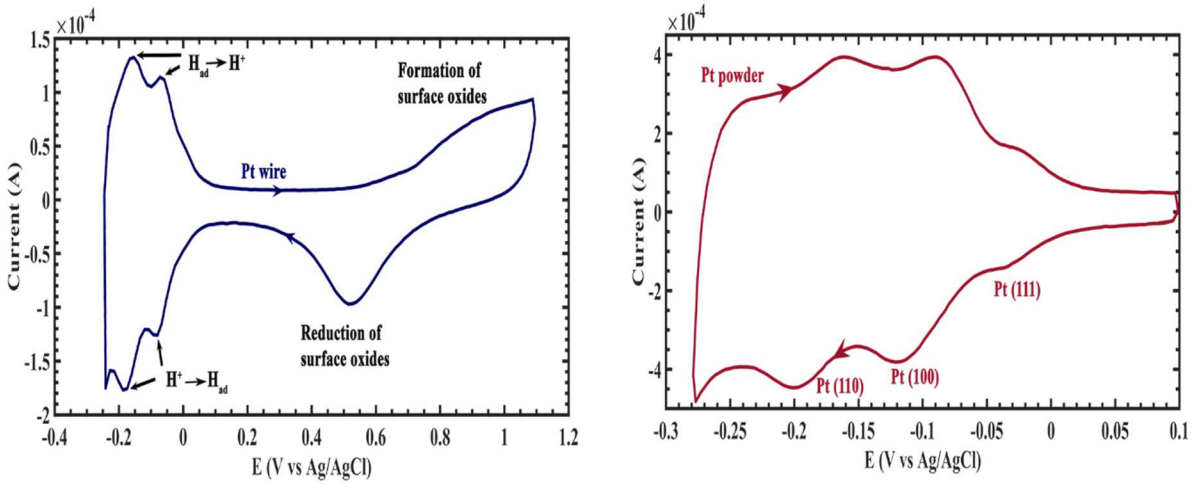

Figure 8. CV of Pt wire at scan rate 200 mV/s (a) and Pt powder (b) at 1 mV/s.

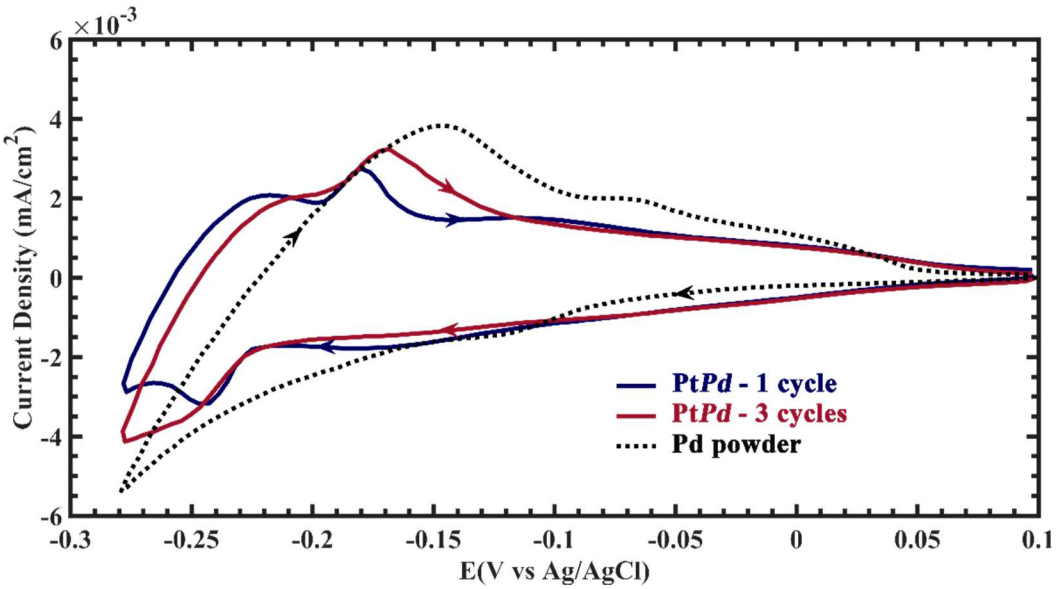

Figure 9. ALED prepared bimetallic Pt*Pd* with 1 cycle and 3 cycles in 0.1 M H_2SO_4 at scan rate 1 mV/s. CV of Pd powder (dotted line).

Figure S1. An Electrochemical cell for CV of Powders.

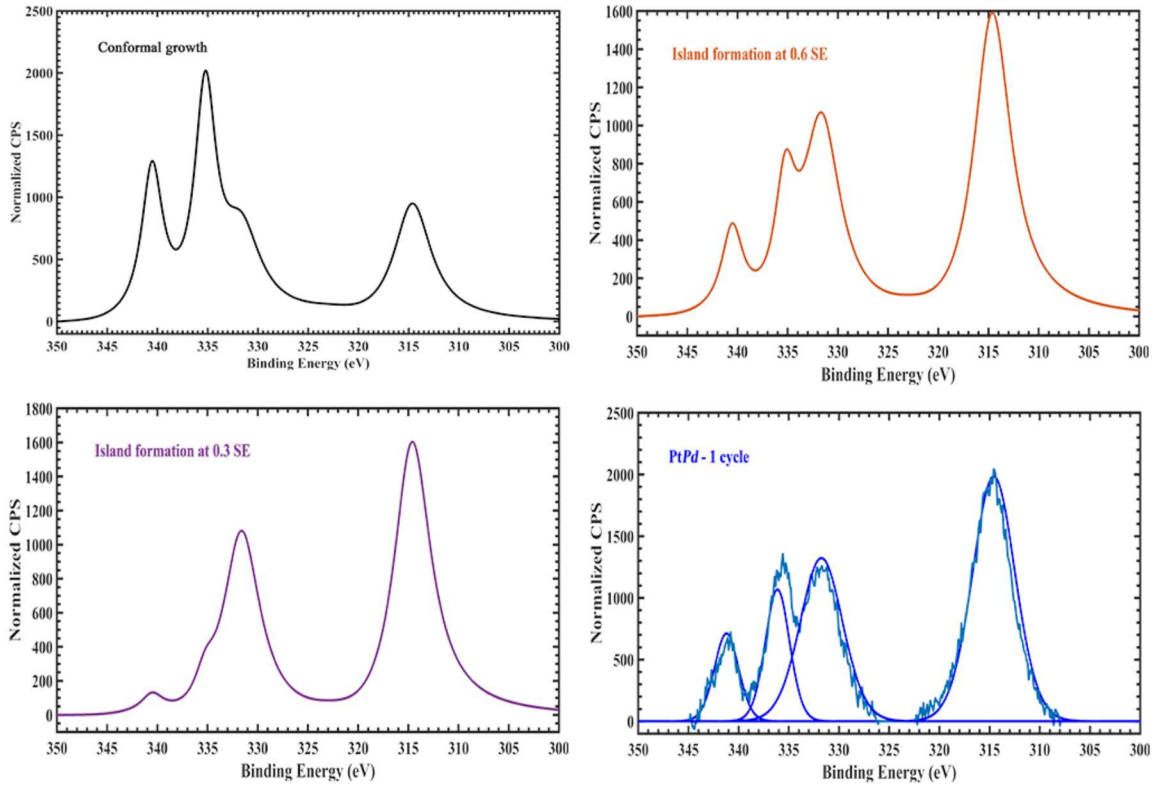

Figure S2. Simulated spectra for three growth models (a-c) and Experimentally observed XPS spectrum of Pt*Pd*- 1 cycle with fitted components (d).